Crossref Similarity Check Powered by iThenticate

Sliding Mode Speed Controller Design for Field Oriented Controlled PMSM Drive of an Electric Vehicle

Hau Huu VO

Modeling Evolutionary Algorithms Simulation and Artificial Intelligence, Faculty of Electrical and Electronics Engineering, Ton Duc Thang University, Ho Chi Minh City, Vietnam

Corresponding Author: Hau Huu Vo (Email: vohuuhau@tdtu.edu.vn)
(Received: 19-May-2023; accepted: 07-Agust-2023; published: 30-Sep-2023)
http://dx.doi.org/10.55579/jaec.202373.414

Abstract. *The paper deals with an application of sliding mode control (SMC) in speed controller of field oriented controlled permanent magnet synchronous motor (PMSM) for a simplified model of an electrical vehicle. For the simplified one, zero-pole elimination method is utilized to design speed controller because of its simplicity. However, the method brings large integral constant time that makes speed response slow. In order to provide fast and robust-to-noise speed one, the SMC method is utilized to replace the zero-pole elimination (ZPE) one. Simulations at wide range of reference speed and load torque are carried out. Performance indices including steady-state error, overshoot and undershoot are employed to assess the speed controller design methods. Evaluated results confirm that the proposed SMC gives smaller performance indices than the ZPE method.*

Keywords

Permanent magnet synchronous motor, Electric Vehicle, field oriented control, sliding mode control

1. Introduction

Electric Vehicles (EVs) are being utilized to replace gasoline-powered ones in order to achieving low-carbon level [1, 2]. Permanent magnet synchronous motors (PMSMs) are widely employed in EVs because of their suitable characteristics such as built-in magnetic field, high start-up torque, small torque ripple. In order to obtain high performance of PMSM drives, field oriented control (FOC) drive strategy were applied [3, 4]. Injecting current harmonic was utilized to enhance maximum motor torque [4]. Space vector pulse width modulation (SVPWM) schemes were integrated into drive strategies to improve responses [5–7]. The SVPWM was utilized to avoid high-level interference and ensure constant switching frequency [6]. Switching diagram minimized switching loss in a field oriented controlled PMSM drive using SVPWM scheme [7].

In order to achieve robust performance of speed control, proportional-integral (PI) controllers were utilized [8–14]. Tuning rules for PI controllers were presented for various process models [8]. The PI parameters were adjusted nonlinearly to get fast response and low overshoot [9]. The fractional-order PI controllers brought high performance for PMSM drive [10]. The zero-pole elimination (ZPE) method was

© 2023 Journal of Advanced Engineering and Computation (JAEC)

applied to enhance PMSM drive performance [11]. The PI control was utilized to observe disturbance for improving performance of the PI speed controller [12]. Fuzzy logic tuned parameters of the PI speed controller in reactive and active power control of PMSM drive to obtain robust steady state and short response time [13]. Auto-coupling PI control gave robustness to disturbance for PMSM servo drive system [14]. Another widely used solution for robust drive performance is sliding mode control (SMC) that owns some advantages such as robustness to load and disturbances, finite-time convergence [15–24].

Variations of the SMC were deployed for applications of control and observation [15]. Two switching functions were used in integral SMC (ISMC) to obtain fast and robust-to-load response [16]. The chattering problem was decreased and the accuracy was guaranteed in ISMC [17]. Discrete SMC was combined with perturbation estimation to get high-performance tracking [18]. The SMC was integrated into model predictive control of PMSM drive for receiving quick and robust response [19]. The chattering problem was eliminated and the drive robustness was ensured by a super-twisting SMC [20]. A terminal SMC reaching law was presented to improve the control performance of the PMSM drive under disturbances [21]. A variation of the SMC reduced the speed error and improved the robustness in the PMSM drive [22]. An adaptive backstepping SMC integrated a disturbance observer was utilized to enhance position accuracy in a PMSM drive [23]. The SMC and a state observer were employed in speed controller to improve speed precision of a PMSM servo system [24]. In next section, the SVPWM-FOC PMSM drive utilizing the ZPE method for design of current controllers are selected to present due to its simplicity. Then, the ZPE and the SMC are utilized to design the speed controllers. The SMC is chosen to provide strong robustness to load activation for the PMSM drive. Simulations and conclusions are carried out in last sections.

2. Sliding mode speed controller for FOC PMSM drive

Fig. 1 presents structure of SVPWM-FOC PMSM drive integrated ZPE or SMC speed controller. Mathematic model [2] of PMSM drive for a simplified electric vehicle is expressed by Eqs.(1)-(6):

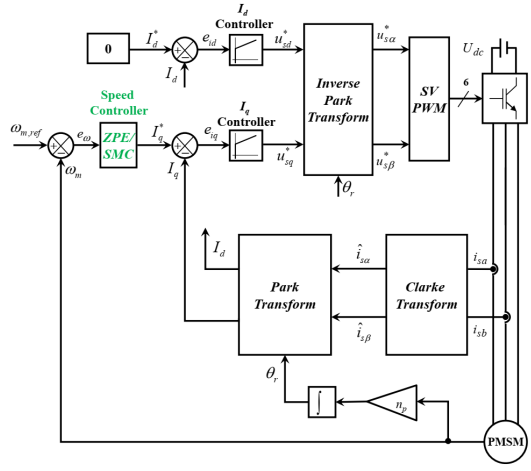

Fig. 1: Structure of SVPWM-FOC PMSM drive integrated ZPE or SMC speed controller.

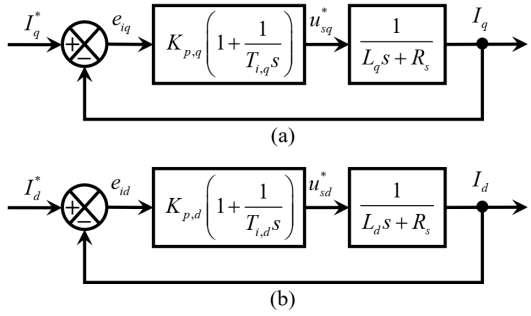

Fig. 2: Simplified control systems of (a) torque-component current I_q; (b) flux-component current I_d.

$$u_{s\alpha} = \frac{d\psi_{s\alpha}}{dt} + R_s i_{s\alpha} \tag{1}$$

$$u_{s\beta} = \frac{d\psi_{s\beta}}{dt} + R_s i_{s\beta} \tag{2}$$

$$\psi_{s\alpha} = L_s i_{s\alpha} + \Phi_M \cos\theta_r \tag{3}$$

$$\psi_{s\beta} = L_s i_{s\beta} + \Phi_M \sin\theta_r \tag{4}$$

$$T_e = \frac{3}{2} n_p (i_{s\beta}\psi_{s\alpha} - i_{s\alpha}\psi_{s\beta}) \tag{5}$$

$$J_m \frac{d\omega_m}{dt} = T_e - T_L - B_m \omega_m \tag{6}$$

where: $u_{s\alpha}$ & $u_{s\beta}$, $\psi_{s\alpha}$ & $\psi_{s\beta}$ and $i_{s\beta}$ & $\psi_{s\alpha}$ are $\alpha-$ and $\beta-$ components of stator voltage vector, stator flux vector, and stator current vector, respectively; R_s & L_s - stator resistance, stator inductance; Φ_M - magnetic flux of the permanent magnet; θ_r - rotor position; n_p - number of pole pairs; J_m - moment of inertia; B_m - rotational damping constant; ω_m - mechanical speed; T_e - motor torque; T_L - load torque. Estimates of stator current components are calculated by Clarke Transform block (see (7)-(8)):

$$\hat{i}_{s\alpha} = i_{sa} \tag{7}$$

$$\hat{i}_{s\beta} = \frac{i_{sa} + 2i_{sb}}{\sqrt{3}} \tag{8}$$

Flux I_d and torque I_q components of stator current vector are computed according to Eqs.(9)-(10) thanks to Park Transform block:

$$I_d = \hat{i}_{s\beta}\sin\theta_r + \hat{i}_{s\alpha}\cos\theta_r \tag{9}$$

$$I_q = -\hat{i}_{s\alpha}\sin\theta_r + \hat{i}_{s\beta}\cos\theta_r \tag{10}$$

Torque-component I_q and flux-component I_d controllers respectively provide references of torque u_{sq} and flux u_{sd} components of stator voltages according to Eqs. (11)-(12):

$$u^*_{sq} = K_{p,q}\left(e_{iq} + \frac{1}{T_{i,q}}\int e_{iq}dt\right) \tag{11}$$

$$u^*_{sd} = K_{p,d}\left(e_{id} + \frac{1}{T_{i,d}}\int e_{id}dt\right) \tag{12}$$

where $K_{p,q}$ & $T_{i,q}$; $K_{p,d}$ & $T_{i,d}$ (see Fig. 2) are respectively proportional gains & integral constant times of PI controllers. With the aim of maximizing the motor torque, reference value of flux-component current is set be zero. Desired stator voltage components are computed by Inverse Park Transform block according to Eqs. (13)-(14):

$$u^*_{s\alpha} = -u^*_{sq}\sin\theta_r + u^*_{sd}\cos\theta_r \tag{13}$$

$$u^*_{s\beta} = u^*_{sd}\sin\theta_r + u^*_{sq}\cos\theta_r \tag{14}$$

And the components are utilized to provide switching diagram of IGBTs in the inverter. In Fig. 2a & Fig. 2b, transfer functions of simplified current control systems are given by Eqs. (15)-(16):

$$G_q(s) = \frac{I_q(s)}{I^*_q(s)} = \frac{K_{p,q}\left(1 + \frac{1}{T_{i,q}s}\right)\frac{1}{L_q s + R_s}}{1 + K_{p,q}\left(1 + \frac{1}{T_{i,q}s}\right)\frac{1}{L_q s + R_s}} \tag{15}$$

$$G_d(s) = \frac{I_d(s)}{I^*_d(s)} = \frac{K_{p,d}\left(1 + \frac{1}{T_{i,d}s}\right)\frac{1}{L_d s + R_s}}{1 + K_{p,d}\left(1 + \frac{1}{T_{i,d}s}\right)\frac{1}{L_d s + R_s}} \tag{16}$$

Utilizing the ZPE method, the current controllers are designed as follows [11]:

$$T_{i,q} = \frac{L_q}{R_s} \tag{17}$$

$$T_{i,d} = \frac{L_d}{R_s} \tag{18}$$

$$K_{p,q} = 2\pi f_{qd} L_q \tag{19}$$

$$K_{p,d} = 2\pi f_{qd} L_d \tag{20}$$

$$f_{dq} = \frac{f_s}{10} \tag{21}$$

where f_s- switching frequency of the inverter, f_{qd} - bandwidth of I_q and I_d currents control loops. The transfer functions are converted into Eqs. (22)-(23):

$$G_q(s) = \frac{1}{(2\pi f_{qd})^{-1}s + 1} \tag{22}$$

$$G_d(s) = \frac{1}{(2\pi f_{qd})^{-1}s + 1} \tag{23}$$

Next, in order to design speed controller, two methods ZPE and SMC are presented.

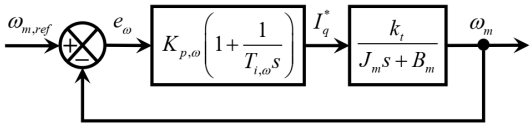

Fig. 3: Simplified motor speed control system.

© 2023 Journal of Advanced Engineering and Computation (JAEC)

For the ZPE method, motor speed control system is simplified as shown in Fig. 3, and its transfer function is given by:

$$G_\omega(s) = \frac{\omega_m(s)}{\omega_{m,ref}(s)} = \frac{K_{p,\omega}\left(1+\frac{1}{T_{i,\omega}s}\right)\frac{k_t}{J_m s+B_m}}{1+K_{p,\omega}\left(1+\frac{1}{T_{i,\omega}s}\right)\frac{k_t}{J_m s+B_m}} \quad (24)$$

where $I_{p,\omega}$ & $T_{j,\omega}$ - proportional gain & integral constant times of the speed controller, and

$$k_t = \frac{K_T}{\sqrt{2}} = \frac{T_N}{\sqrt{2}I_N} \quad (25)$$

where T_N - rated torque, I_N - rated current, K_T - torque constant. The ZPE method is applied for the simplified motor speed control system as follows [11]:

$$T_{i,\omega} = \frac{J_m}{B_m} \quad (26)$$

$$K_{p,\omega} = 2\pi f_\omega J_m k_t \quad (27)$$

$$f_\omega = \frac{f_s}{100} \quad (28)$$

where f_ω - bandwidth of speed control loop. The transfer function of the speed control system is converted into Eq. (29) thanks to Eqs. (26)-(27):

$$G_\omega(s) = \frac{1}{(2\pi f_\omega)^{-1}s+1} \quad (29)$$

For the SMC method, switching function S and its time derivative are defined as follows [25]:

$$S = K_{p,sw}\left(e_\omega + \frac{1}{T_{i,sw}}\int e_\omega dt\right) \quad (30)$$

$$\dot{S} = K_{p,sw}\left(\dot{e}_\omega + \frac{e_\omega}{T_{i,sw}}\right) \quad (31)$$

where $K_{p,s\omega}$ & $K_{i,s\omega}$ - proportional gain & integral constant time of the switching function, and

$$e_\omega = \omega_{m,ref} - \omega_m \quad (32)$$

Lyapunov function L_f and its time derivative are chosen as follows:

$$L_f = \frac{S^2}{2} \quad (33)$$

$$\dot{L}_f = S\dot{S} \quad (34)$$

In order to obtain the stability of the motor speed control system, the time derivative of the switching function is selected as follows:

$$\dot{S} = -k_{s,sw}sign(S) \quad (35)$$

where $k_{s,s\omega}$ >0. With assumption of $\omega_{m,ref}$ = const, substitute Eq. (6) into Eq. (31) to obtain Eq. (36):

$$\dot{S} = K_{p,sw}\left(\frac{T_L + B_m\omega_m - T_e}{J_m} + \frac{e_\omega}{T_{i,sw}}\right) \quad (36)$$

The motor torque is derived by substituting the time derivative of the switching function in Eq. (35) into Eq. (36):

$$T_e = T_L + B_m\omega_m + J_m\left(\frac{k_{s,sw}sign(S)}{K_{p,sw}} + \frac{e_\omega}{T_{i,sw}}\right) \quad (37)$$

Output of speed controller is derived by approximating reference torque as motor torque:

$$I_q^* = \frac{T_e^*}{K_T} \quad (38)$$

$$I_q^* = \frac{T_L + B_m\omega_m + J_m\left(\frac{k_{s,sw}sign(S)}{K_{p,sw}} + \frac{e_\omega}{T_{i,sw}}\right)}{K_T} \quad (39)$$

Load torque is considered noise because of its inaccurate information. The control output and reference torque is approximated as follows:

$$I_q^* = \frac{B_m\omega_m + J_m\left(\frac{k_{s,sw}sign(S)}{K_{p,sw}} + \frac{e_\omega}{T_{i,sw}}\right)}{K_T} \quad (40)$$

$$T_e^* = B_m\omega_m + J_m\left(\frac{k_{s,sw}sign(S)}{K_{p,sw}} + \frac{e_\omega}{T_{i,sw}}\right) \quad (41)$$

Approximate motor torque in Eq. (36) by reference torque in (40) and convert Eq. (36) to obtain Eq. (41):

$$\dot{S} = K_{p,sw}\frac{T_L}{J_m} - k_{s,sw}sign(S) \quad (42)$$

In order to guarantee the stability of the motor speed control system, the $k_{s,s\omega}$ is selected as

follows:

$$k_{s,sw} = \begin{cases} K_{p,sw}\frac{T_L}{J_m} + \varepsilon, & if \quad S > 0 \\ unchanged, & if \quad S = 0 \\ -K_{p,sw}\frac{T_L}{J_m} + \varepsilon, & if \quad S < 0 \end{cases} \tag{43}$$

where $\omega > 0$. Load torque in Eq. (43) is estimated thanks to Eq. (6):

$$T_{L,est} = T_{e,est} - B_m\omega_m - J_m\frac{d\omega_m}{dt} \tag{44}$$

where $T_{e,est}$ - estimated motor torque is given by Eq. (45):

$$T_{e,est} = \frac{3}{2}n_p\Phi_M I_q \tag{45}$$

3. Simulations

The PMSM parameters utilized in simulations are shown in Table 1 Simulations for ZPE and SMC method are presented at $\omega_{m,ref} = (10rpm, 100rpm, 1000rpm)$, load torque is activated at 1 second time with $T_L = (0.1T_N, 0.5T_N, 0.9T_N)$. Switching frequency of the SVPWM is 20kHz. Limitations of outputs of current controllers and speed controller, are respectively ±255V, ±21.1A. Motor speed responses are shown in Figs. 4-12. Table 2 indicates that the SMC brings almost zero overshoot in duration 0.0s-1.0s, while the ZPE provides small overshoot and the value gets bigger as reference speed increases. Undershoot in duration 1.0s-2.0s for the ZPE method is insignificantly larger than the one for the SMC method (see Table 3), and it is greater under higher load and reference speed. Especially, steady-state er-

Tab. 1: Parameters of PMSM [26].

Quantity	Symbol	Value
rated torque	T_N	12.5 Nm
rated current	I_N	14.9 A
rated voltage	U_N	180 V
rated power	P_N	3.9 kW
magnetic flux of the permanent magnet	Φ_M	0.185 Wb
moment of inertia	J_m	0.0755 kgm2
rotational damping constant	B_m	10-3Nm.s
rated speed	n_N	3000 rpm
number of pole pairs	n_p	3
stator resistance	R_s	0.3 W
q-axis inductance	L_q	8.5 mH
d-axis inductance	L_d	8.5 mH

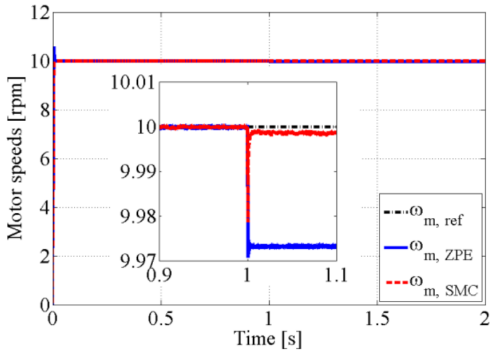

Fig. 4: Simplified motor speed control system.

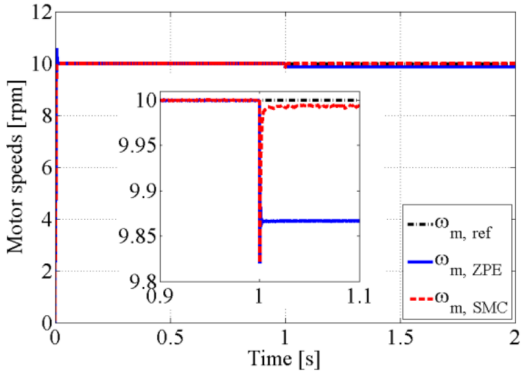

Fig. 5: Simplified motor speed control system.

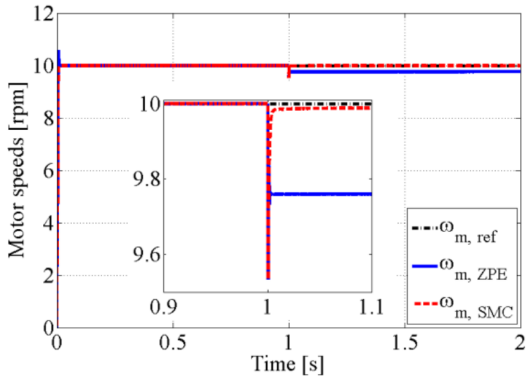

Fig. 6: Motor speeds at $\omega_{ref} = 10$rpm, $T_L = 0.9T_N$.

© 2023 Journal of Advanced Engineering and Computation (JAEC)

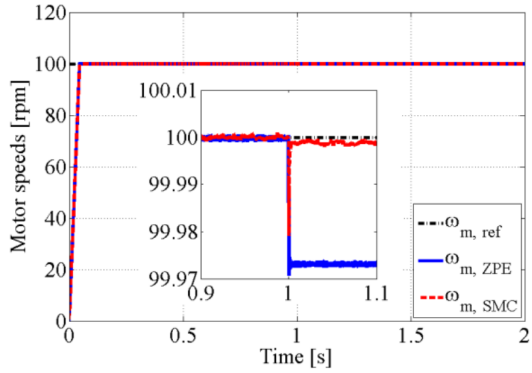

Fig. 7: Motor speeds at $\omega_{ref} = 100$rpm, $T_L = 0.1T_N$.

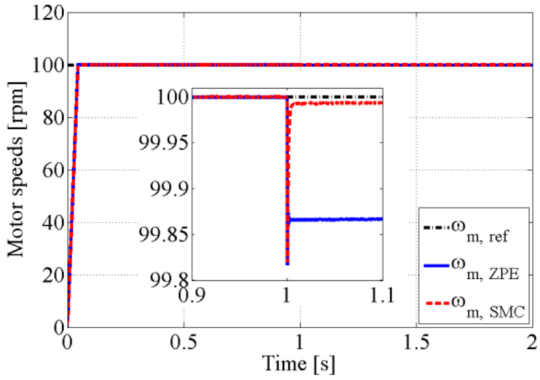

Fig. 8: Motor speeds at $\omega_{ref} = 100$rpm, $T_L = 0.5T_N$.

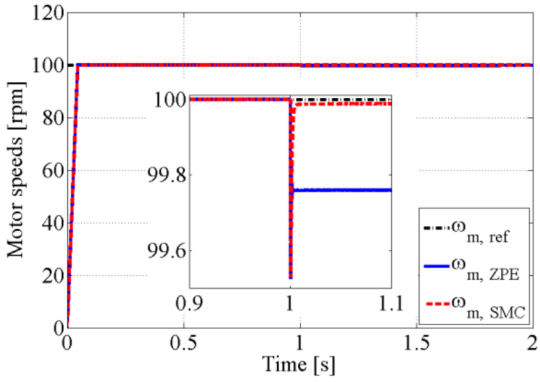

Fig. 9: Motor speeds at $\omega_{ref} = 100$rpm, $T_L = 0.9T_N$.

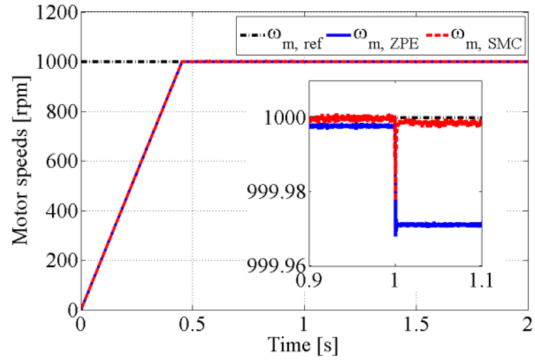

Fig. 10: Motor speeds at $\omega_{ref} = 1000$rpm, $T_L = 0.1T_N$.

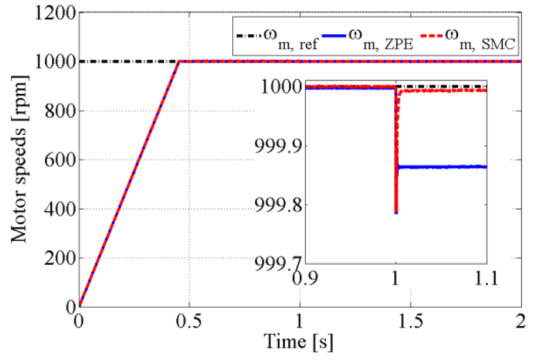

Fig. 11: Motor speeds at $\omega_{ref} = 1000$rpm, $T_L = 0.5T_N$.

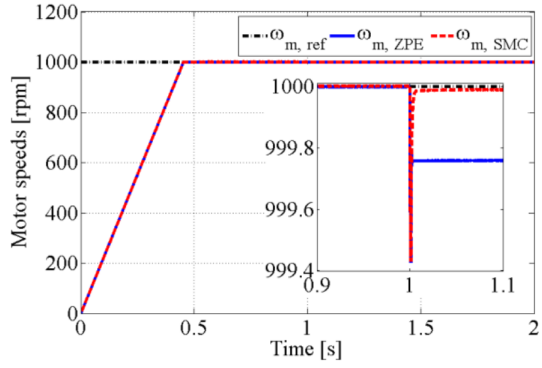

Fig. 12: Motor speeds at $\omega_{ref} = 1000$rpm, $T_L = 0.9T_N$.

ror for the SMC is 15.2-25.4 times lower than the one for the ZPE (see Table 4). Reason for this is the ZPE owns long integral constant time $T_{i,\omega}$ due to small rotational damping constant B_m. On the other hand, the SMC possesses high robustness-to-load-activation which is expressed in a smaller value $I_{q,max,act}$ than the ZPE, where $I_{q,max,act}$ - peak value of torque-current component I_q after load activation by $T_L = 0.9T_N$ (see Figs. 13-15 and Table 5).

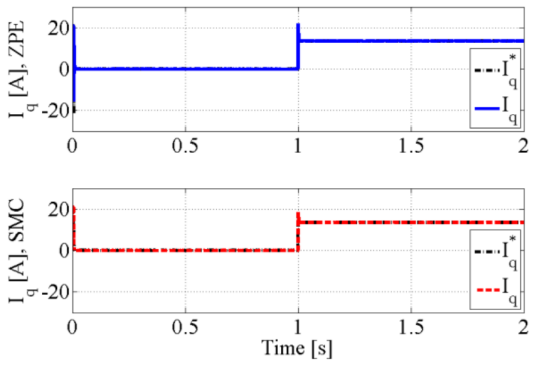

Fig. 13: Torque-component current I_q at ω_{ref} = 10rpm, $T_L = 0.9T_N$.

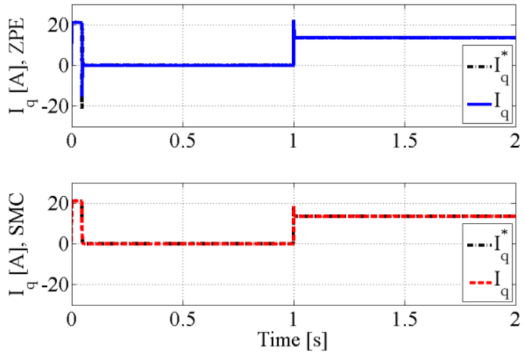

Fig. 14: Torque-component current I_q at ω_{ref} = 100rpm, $T_L = 0.9T_N$.

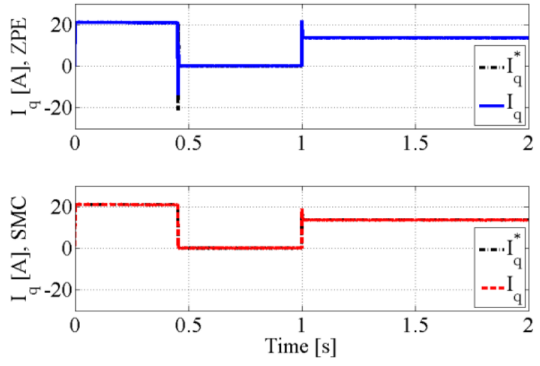

Fig. 15: Torque-component current I_q at ω_{ref} = 1000rpm, $T_L = 0.9T_N$.

Tab. 2: Overshoot [%] in duration 0.0s-1.0s.

Method	w_{ref}= 10	w_{ref}= 100	w_{ref}= 1000
ZPE	5.88	0.56	0.04
SMC	0	0	0

Tab. 3: Undershoot [%] in duration 1.0s-2.0s.

w_{ref}	T_L	ZPE	SMC
10rpm	$0.1T_N$	0.29	0.21
	$0.5T_N$	1.8	1.79
	$0.9T_N$	4.66	4.66
100rpm	$0.1T_N$	0.029	0.021
	$0.5T_N$	0.184	0.18
	$0.9T_N$	0.474	0.47
1000rpm	$0.1T_N$	0.0032	0.0023
	$0.5T_N$	0.0215	0.0212
	$0.9T_N$	0.0572	0.057

Tab. 4: Steady-state error [%].

w_{ref}	T_L	ZPE	SMC
10rpm	$0.1T_N$	0.26	0.017
	$0.5T_N$	1.32	0.069
	$0.9T_N$	2.37	0.12
100rpm	$0.1T_N$	0.027	0.0014
	$0.5T_N$	0.132	0.0059
	$0.9T_N$	0.237	0.0112
1000rpm	$0.1T_N$	0.0028	0.00011
	$0.5T_N$	0.0135	0.00069
	$0.9T_N$	0.0239	0.00123

Tab. 5: Peak value $I_{q,max,act}$ [A] after activation by T_L = $0.9T_N$.

Method	w_{ref}= 10rpm	w_{ref}= 100rpm	w_{ref}= 1000rpm
ZPE	22.05	22.12	21.89
SMC	18.49	18.37	19.12

4. Conclusions

The ZPE and the SMC speed controllers in the drive structure utilizing SVPWM-FOC for PMSM of a simplified electric vehicle were presented. Simulations and evaluations were carried out at different reference speeds and wide load torque range. The design of the SMC speed controller ensures the Lyapunov stability of the

© 2023 Journal of Advanced Engineering and Computation (JAEC)

PMSM drive, resulting in high robustness-to-load-activation. The SMC decreases the steady-state error by 93% at least compared to the ZPE for evaluated cases. It also gives almost zero overshoot at starting and its response is more robust under load activation than the ZPE. Super-twisting or high-order SMC methods or disturbance observers can be employed to extend the robustness of the speed controller. In order to reduce chattering phenomena, a low-pass filter and a modified integral sliding variable can be utilized [27]. In order to expand operating speed range higher than the rated speed, flux-weakening strategy using vector current control based on regulating modulus of applied voltage can be integrated into the drive structure with the proposed SMC [28].

References

[1] Bose, B. (2013). Global Energy Scenario and Impact of Power Electronics in 21st Century. *IEEE Transactions on Industrial Electronics*, *60*, 2638–2651.

[2] Boumegouas, M. & Kouzi, K. (2022). A New Synergetic Scheme Control of Electric Vehicle Propelled by Six-phase Permanent Magnet Synchronous Motor. *Advances in Electrical and Electronic Engineering*, *20*, 1–14.

[3] Blaschke, F. (1972). The Principle of Orientation as Applied to the New Transvektor Closed–Loop Control System for Rotating-Field Machines. *Siemens Review*, *34*, 217–220.

[4] Slunjski, M., Stiscia, O., Jones, M., & Levi, E. (2021). General Torque Enhancement Approach for a Nine-Phase Surface PMSM with Built-In Fault Tolerance. *IEEE Transactions on Industrial Electronics*, *68*, 6412–6423.

[5] Bose, B. (2022). Modern Power Electronics and AC Drives. Prentice Hall. *Prentice Hall*.

[6] Brandstetter, P., Kuchar, M., Vo, H., & Dong, C. (2017). Induction motor drive with PWM direct torque control. *Proceedings of the 2017 18th International Scientific Conference on Electric Power Engineering (EPE), Kouty nad Desnou, Czech Republic*, 409–413.

[7] Yao, H., Shi, Y., Wang, T., & Xia, C. (2021). A Novel SVPWM Scheme for Field-Oriented Vector-Controlled PMSM Drive System Fed by Cascaded H-Bridge Inverter. *IEEE Transactions on Power Electronics*, *36*, 8988–9000.

[8] Dwyer, O. (2009). Handbook of PI and PID Controller Tuning Rules. *Imperial College Pres*.

[9] Zhihong, W., Gensheng, L., Yuan, Z., Guangyu, T., & L., K. (2010). A New Nonlinear PI Controller of Permanent Magnet Synchronous Motor. *Proceedings of 2010 Second International Conference on Intelligent Human-Machine Systems and Cybernetics, Nanjing, China*, 99–102.

[10] Thaka, U., Joshi, V., & Vyawahare, V. (2017). Design of fractional-order PI controllers and comparative analysis of these controllers with linearized, nonlinear integer-order and nonlinear fractional-order representations of PMSM. *International Journal of Dynamics and Contro*, *5*, 187–197.

[11] Hsieh, M., Chen, N., & Ton, T. (2019). System Response of Permanent Magnet Synchronous Motor Drive Based on SiC Power Transistor. *Proceedings of 2019 IEEE 4th International Future Energy Electronics Conference (IFEEC)*, 1–6.

[12] Sarsembayev, B., Suleimenov, K., & Do, T. (2021). High Order Disturbance Observer Based PI-PI Control System with Tracking Anti-Windup Technique for Improvement of Transient Performance of PMSM. *IEEE Access*, *9*, 66323–66334.

[13] Khanh, P. & Anh, H. (2023). Improved PMSM Speed Control Using Fuzzy PI Method for Hybrid Active and Reactive Power Control Approach. *Proceedings of the Computational Intelligence Methods for*

Green Technology and Sustainable Development GTSD 2022, Lecture Notes in Networks and Systems, *567*, 345–356.

[14] Zhang, Z., Zeng, Z., Huang, L., & Wang, W. (2023). Auto-coupling PI Controller of PMSM Speed Servo System. *roceedings of the 17th Annual Conference of China Electrotechnical Society ACCES 2022, Lecture Notes in Electrical Engineering*, *1012*, 654–661.

[15] Shtessel, Y., Edwards, C., Fridman, L., & Levant, A. (2014). Sliding Mode Control and Observation. *Birkhäuser Base*.

[16] Dong, C., Brandstetter, P., Vo, H., Tran, T., & Vo, D. (2017). Adaptive Sliding Mode Controller for Induction Motor. *Proceedings of the AETA 2016: Recent Advances in Electrical Engineering and Related Sciences AETA 2016, Lecture Notes in Electrical Engineering*, *415*, 543–553.

[17] Pan, Y., Yang, C., Pan, L., & Yu, H. (2018). Integral Sliding Mode Control: Performance, Modification, and Improvement. *IEEE Transactions on Industrial Informatics*, *14*, 3087–3096.

[18] Huynh-Van, V. & Tran-Thanh, P. (2019). Discrete Sliding Mode Control Design for Piezoelectric Actuator. *Journal of Advanced Engineering and Computation*, *3*, 492–502.

[19] Guo, Q. & Pan, T. (2020). A Predictive Speed Control Method Based on Sliding Mode Model for PMSM Drive System. *Proceedings of 2019 Chinese Intelligent Automation Conference CIAC 2019, Lecture Notes in Electrical Engineering*, *586*, 512–520.

[20] Balaji, K. & Kumar, R. (2020). Adaptive Super-Twisting Sliding Mode Controller-Based PMSM Fed Four Switch Three Phase Inverter. *Proceedings of the Intelligent Computing in Engineering, Advances in Intelligent Systems and Computing*, *1125*, 327–337.

[21] Junejo, A., Xu, W., Mu, C., Ismail, M., & Liu, Y. (2020). Adaptive Speed Control of PMSM Drive System Based a New Sliding-Mode Reaching Law. *IEEE Transactions on Power Electronics*, *35*, 12110–12121.

[22] Ma, Y., Li, D., Li, Y., & Yang, L. (1922). Novel Discrete Compound Integral Terminal Sliding Mode Control with Disturbance Compensation for PMSM Speed System. *IEEE/ASME Transactions on Mechatronics*, *27*, 549–560.

[23] Nguyen, T., Nguyen, T., Le, K., Tran, H., & Jeon, J. (2023). An Adaptive Backstepping Sliding-Mode Control for Improving Position Tracking of a Permanent-Magnet Synchronous Motor with a Nonlinear Disturbance Observer. *IEEE Access*, *11*, 19173–19185.

[24] Li, H., Yang, S., & Le, Y. (2023). Torque Ripple Minimization of Low-Speed Gimbal Servo System Using Parameter-Optimized ESO. *IEEE Journal of Emerging and Selected Topics in Power Electronics*, *11*, 2094–2103.

[25] Vo, H., Tran, D., Thieu, T., Le, A., Dong, C., & P., B. (2021). Sliding Mode PWM-Direct Torque Controlled Induction Motor Drive with Kalman Filtration of Estimated Load. *Journal of Advanced Engineering and Computation*, *5*, 265–276.

[26] Daud, A., Alsayid, B., & Zaidan, A. (2012). DSP Based Simulator for Field Oriented Control of the Surface Permanent Magnet Synchronous Motor Drive. *International Journal of Circuits, Systems and Signal Processing*, *6*, 29–37.

[27] Pan, Y., Yang, C., Pan, L., & Yu, H. (2018). Integral Sliding Mode Control: Performance, Modification, and Improvement. *IEEE Transactions on Industrial Informatics*, *14*, 3087–3096.

[28] Miguel-Espinar, C., Heredero-Peris, D., Villafafila-Robles, R., & Montesinos-Miracle, D. (2023). Review of Flux-Weakening Algorithms to Extend the Speed Range in Electric Vehicle Applications With Permanent Magnet Synchronous Machines. *IEEE Access*, *11*, 22961–22981.

 © 2023 Journal of Advanced Engineering and Computation (JAEC)

About Authors

Hau Huu VO hold a PhD degree from Technical University of Ostrava (VSB-TUO), Czech Republic in 2017. He has been working as a Lecturer at Faculty of Electrical and Electronics Engineering (FEEE), Ton Duc Thang University (TDTU) since 2010. His research interests are applications of control techniques for electrical drives.

"This is an Open Access article distributed under the terms of the Creative Commons Attribution License, which permits unrestricted use, distribution, and reproduction in any medium provided the original work is properly cited (CC BY 4.0)."